Cerebral Cortex February 2016;26:517–529
doi:10.1093/cercor/bhu204
Advance Access publication September 9, 2014

Top-down Modulation of Neural Activity in Anticipatory Visual Attention: Control Mechanisms Revealed by Simultaneous EEG-fMRI

Yuelu Liu[1,2], Jesse Bengson[2], Haiqing Huang[1], George R. Mangun[2,3] and Mingzhou Ding[1]

[1]J. Crayton Pruitt Family Department of Biomedical Engineering, University of Florida, Gainesville, FL 32611, USA, [2]Center for Mind and Brain, University of California, Davis, Davis, CA 95618, USA and [3]Departments of Psychology and Neurology, University of California, Davis, Davis, CA 95616, USA

Address correspondence to Mingzhou Ding, The J. Crayton Pruitt Family Department of Biomedical Engineering, J-285 Biomedical Sciences Building, PO Box 116131, University of Florida, Gainesville, FL 32611, USA. Email: mding@bme.ufl.edu

In covert visual attention, frontoparietal attention control areas are thought to issue signals to selectively bias sensory neurons to facilitate behaviorally relevant information and suppress distraction. We investigated the relationship between activity in attention control areas and attention-related modulation of posterior alpha activity using simultaneous electroencephalography (EEG) and functional magnetic resonance imaging in humans during cued visual-spatial attention. Correlating single-trial EEG alpha power with blood-oxygen-level dependent (BOLD) activity, we found that BOLD in the intraparietal sulcus (IPS) and left middle frontal gyrus was inversely correlated with occipital alpha power. Importantly, in IPS, inverse correlations were stronger for alpha within the hemisphere contralateral to the attended hemifield, implicating the IPS in the enhancement of task-relevant sensory areas. Positive BOLD-alpha correlations were observed in sensorimotor cortices and the default mode network, suggesting a mechanism of active suppression over task-irrelevant areas. The magnitude of cue-induced alpha lateralization was positively correlated with BOLD in dorsal anterior cingulate cortex and dorsolateral prefrontal cortex, implicating a role of executive control in attention. These results show that IPS and frontal executive areas are the main sources of biasing influences on task-relevant visual cortex, whereas task-irrelevant default mode network and sensorimotor cortex are inhibited during visual attention.

Keywords: alpha oscillations, anterior cingulate cortex, dorsal attention network, simultaneous EEG-fMRI, visuospatial attention

Introduction

Our ability to selectively focus attention is a core cognitive ability (Posner 1980). Extensive research on visual selective attention has demonstrated that sensory signals are strongly modulated by attention at various stages of the visual pathways (Van Voorhis and Hillyard 1977; Moran and Desimone 1985; Heinze et al. 1994; Chelazzi et al. 1998; Tootell et al. 1998; O'Connor et al. 2002; Briggs et al. 2013). Most models of visual attention posit that this modulation of visual processing is under the control of a frontoparietal attention network whose top-down influences alter the gain of signals in multiple visual areas (Mesulam 1999; Corbetta and Shulman 2002; Miller and Buschman 2013). Evidence for such models comes from observations of attentional deficits following focal brain damage (Mesulam 1981; Barcelo et al. 2000), spatially specific changes in the background neural activity (single neuron spikes, blood-oxygen-level dependent [BOLD] signals, and electroencephalography [EEG] alpha activity) in visual cortex during preparatory attention (Luck et al. 1997; Kastner et al. 1999; Hopfinger et al. 2000; Worden et al. 2000; Thut et al. 2006), and modulations of visual cortical activity by stimulation in the frontal and parietal cortex (Hilgetag et al. 2001; Moore and Armstrong 2003; Moore and Fallah 2004; Hung et al. 2005; Thut et al. 2005; Szczepanski et al. 2010).

The modulation of posterior alpha oscillations (8–12 Hz) following an attentional cue is one robust neural marker signifying selective sensory biasing by covert attention via top-down mechanisms. When covert attention is directed to one side of the visual field, alpha oscillation is more strongly suppressed over the hemisphere contralateral to the attended hemifield (Worden et al. 2000; Sauseng et al. 2005; Thut et al. 2006; Rajagovindan and Ding 2011). This lateralized reduction of alpha activity is thought to reflect an increase in cortical excitability in task-relevant sensory neurons to facilitate the processing of upcoming stimulus inputs (Sauseng et al. 2005; Thut et al. 2006; Romei et al. 2008). Putative sources of the top-down control signals include the dorsal frontoparietal attention network, and other higher-order executive regions known to mediate goal-directed behaviors (Kastner et al. 1999; Corbetta et al. 2000; Hopfinger et al. 2000; Capotosto et al. 2009; Corbetta and Shulman 2011). Two recent studies employing repetitive transcranial magnetic stimulation (rTMS) showed disrupted alpha lateralization after selectively disrupting processing in the frontal eye field (FEF) and intraparietal sulcus (IPS) (Capotosto et al. 2009, 2012), providing strong evidence of the functional link between activity in the frontoparietal network and modulation of posterior alpha activity. Evidence from testing that does not perturb neural activity, however, has remained scarce.

The simultaneous recording of EEG and functional magnetic resonance imaging (fMRI) opens avenues to address this gap. In the present study, we recorded simultaneous EEG-fMRI from subjects performing a cued visual-spatial attention task. Correlating single-trial alpha power and alpha lateralization during the post-cue period with BOLD activity across the entire brain, we sought to identify sources responsible for different aspects of attention-related alpha modulation, and to establish additional evidence for direct interactions between frontoparietal control systems and visual cortical activity during anticipatory attention. We also investigated the involvement of other brain structures known to mediate goal-directed behavior, such as the dorsal anterior cingulate cortex (dACC) (Crottaz-Herbette and Menon 2006; Dosenbach et al. 2006).

Materials and Methods

Participants

Eighteen right-handed college students with normal or corrected-to-normal vision, and no history of neurological or psychiatric disorders, participated in the study in exchange for course credit. The

experimental protocol was approved by the Institutional Review Board of the University of Florida. Written informed consent was obtained from every participant before the experiment. Data from 5 participants were excluded for one of the following 3 reasons: (1) behavioral performance below criterion (1 participant); (2) difficulties in following task instructions (1 participant); and (3) excessive body or eye movements (3 participants). The remaining 13 participants (5 females) had a mean age of 19 years (SD = 1.34 years).

Paradigm

Stimuli were displayed on a 30-in. MR-compatible LCD monitor with 60-Hz refresh rate that was placed outside of the scanner bore beyond the head of the subject. Participants viewed the stimuli via a mirror at a viewing distance of ~230 cm. Within an experimental block, participants were instructed to maintain constant fixation on a white dot positioned at the center of a gray background. Two additional dots were placed at the lower left and lower right peripheral visual fields (5° lateral to the central fixation and 1.2° below the horizontal meridian) to continuously mark the 2 locations where task-relevant or irrelevant stimuli would appear.

As illustrated in Figure 1, each trial began with a 200 ms duration symbolic cue presented slightly above the central fixation point, which instructed the participants to covertly direct their attention (not their eyes) to either the lower left or lower right visual field. Left-directing cues and right-directing cues had equal probability. Following a variable cue-target interval randomized between 2000 and 8000 ms, target stimuli composed of vertical black-and-white gratings (100% contrast; 1.7° in viewing angle) were flashed briefly for 100 ms at one of the marked peripheral locations with equal probability (50% target validity). When a target stimulus appeared at the cued (attended) spatial location, participants were required to discriminate the spatial frequency (5.5 vs. 5.0 cycles per degree) of the grating and make a speeded 2-button choice response using their right index or middle fingers without sacrificing accuracy. Stimuli occurring at the unattended location were to be ignored. The difficulty in discriminating the 2 grating patterns, which had very similar spatial frequencies, strongly encouraged the deployment and maintenance of covert attention following the cue.

It should be noted that the instructional cueing strategy used here differs slightly from the probabilistic cueing method used in classical visuospatial attention paradigms (e.g., Posner 1980) because it does not require responses for stimuli at uncued locations, and therefore does not yield behavioral measures of selective attention. We have employed this instructional cue approach previously (e.g., Hopf and Mangun 2000; Hopfinger et al. 2000; Walsh et al. 2011), as have other investigators (e.g., Worden et al. 2000; Kelly et al. 2009), because it engenders strongly focused attention. In a control behavioral study in the scanner, however, we tested our design using probabilistic cueing with the same stimuli and presentation schedule and obtained behavioral measures of target processing at both the cued- and uncued-location. In addition, we incorporated a divided attention decrement test where the cue instructed the subjects to divide attention between left and right field locations (Navon and Gopher 1979). We observed the standard attention effects in reaction time (RT): responses to cued targets were significantly faster than those in the divided attention condition ($P < 0.01$) or the uncued condition ($P < 0.03$). Therefore, the speeded discrimination task was sufficiently difficult to require focal attention to achieve maximal performance.

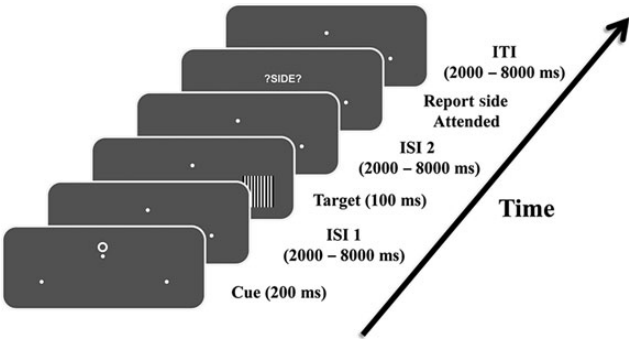

Figure 1. An illustration of the sequence of events within a trial. Following cue onset, participants covertly directed their attention toward either left or right hemifield marked by the 2 white dots, while maintaining eye fixation on the central dot. Targets were flashed briefly at one of the marked locations after a variable inter-stimulus interval. Participants were required to discriminate the spatial frequency of the gratings and make a forced 2-button choice response only when targets appeared on the attended location. At the end of each trial, participants were also prompted to report the hemifield they attended to. This reporting was necessitated by another condition of the experiment where the participants, upon seeing a "choice cue," spontaneously decided which side to attend. Data from this choice condition was not analyzed here.

In addition to the 2 types of instructional cues (attend-left versus attend-right), there was a third type of cue (choice cue) randomly inserted in the trial sequence of the experiment, but this condition was not analyzed with respect to the main question of interest in the present study. Nonetheless, we provide the details so all aspects of the design are reported. Upon seeing the choice cue, participants were asked to spontaneously decide which spatial location to attend and then covertly attended the chosen location. The target discrimination task performed in the choice trials was the same as that in the instructional trials. As noted above, these trials were not analyzed for the present study (see Bengson et al. 2014 for additional details of the full design).

Regardless of cue type (cued or choice), following the target stimulus by a random interval of 2000–8000 ms, participants were further prompted by the screen "?SIDE?" to report the spatial location they attended within the trial via a button press (index finger: left, middle finger: right). After reporting where they had attended for that trial, an intertrial interval (ITI) randomized between 2000 and 8000 ms elapsed before the start of the next trial. Bilaterally symmetric symbols were used as cues (T, O, and ◊), and were counterbalanced across subjects as to their meaning (attend-left, attend-right, or freely choose).

All participants went through a training session before the actual experiment to ensure adequate performance (above 70% accuracy) and proper maintenance of eye fixation. The experimental session was divided into multiple blocks of trials, with the length of each block kept around 6 min to prevent subject fatigue. Each participant completed between 8 and 12 blocks for the experiment. A short break was administered between 2 adjacent blocks. The meaning of cues and the importance of proper maintenance of eye fixation were emphasized during each break.

EEG Acquisition and Preprocessing

Continuous EEG data were collected during the experiment with a 32-channel MR-compatible EEG recording system (Brain Products, Germany). Thirty-one Ag/AgCl electrodes were placed on the scalp according to the 10–20 system using an elastic cap. One additional electrode was placed on the subject's upper back to record the electrocardiogram (ECG), which was subsequently used to remove the ballistocardiogram (BCG) artifact during EEG preprocessing. The impedance from scalp channels was kept <5 kΩ throughout the experiment. Referenced to site FCz during recording, the EEG data were bandpass filtered between 0.1 and 250 Hz, sampled at 5000 samples per second, and synchronized with the scanner's internal clock, a step important for the proper removal of the gradient artifacts in subsequent data processing.

The initial EEG preprocessing was performed in BrainVision Analyzer 2.0 (Brain Products, Germany). Gradient and the BCG artifacts were corrected according to a modified version of the average artifact subtraction method proposed in Allen et al. (1998, 2000). Specifically, the gradient artifacts were corrected by constructing an average artifact template over 41 consecutive volumes in a sliding-window fashion, and then subtracting this template from the raw EEG data for each volume. The BCG artifacts were removed using a similar approach in which ECG R-waves were first detected, and 21 consecutive ECG segments defined around the R-waves were averaged to produce a BCG artifact template. The resulting artifact template was then subtracted from EEG data to correct for BCG contamination. The MR-corrected EEG data were then bandpass filtered from 0.1 to 50 Hz, and down

sampled to 250 Hz before being exported to EEGLAB (Delorme and Makeig 2004) for further analyses.

The continuous EEG data were epoched from 500 ms before to 1500 ms after cue onset separately for the attend-left and attend-right trials. Only trials with correct responses were included. Epochs were visually inspected for artifact contamination and trials containing excessive body movement-related artifacts were rejected. Frontal channels (channels FP1, FP2, F7, and F8) were further used to monitor subjects' eye movements and blinks. Epochs contaminated by eye movements as indicated by electro-oculograms recorded from anterior and lateral frontal channels were rejected. We further removed epochs during which subjects blinked within a 200 ms window around cue onset. Across subjects, the mean trial rejection rate was 9.5%, and the mean number of artifact-free trials was 67 and 66 for attend-left and attend-right conditions, respectively. Further EEG preprocessing using Second-Order Blind Identification (Belouchrani et al. 1993) was applied to correct for any residual BCG, eye-blinking, and movement-related artifacts. To sharpen spatial localization, the artifact-free scalp voltage data were converted into reference-free current source density (CSD) data by calculating the 2D spatial Laplacian (Mitzdorf 1985; Chen et al. 2011).

FMRI Acquisition and Preprocessing

MR images were acquired using a 3T Philips Achieva scanner (Philips Medical Systems, the Netherlands) equipped with a 32-channel head coil. Functional images were collected during the experimental sessions using an echo-planar imaging (EPI) sequence with the following scanning parameters: repetition time (TR), 1.98 s; echo time, 30 ms; flip angle, 80°; field of view, 224 mm; slice number, 36; voxel size, 3.5 × 3.5 × 3.5 mm; matrix size, 64 × 64. The slices were oriented parallel to the plane connecting the anterior and posterior commissures. Image acquisition was performed during the initial 1.85 s within each EPI volume, leaving an interval of 130 ms towards the end of each TR where no image acquisition was performed; the absence of gradient artifacts in this interval enables online visual monitoring of the simultaneous EEG acquisition.

MRI data were processed in SPM5 (http://www.fil.ion.ucl.ac.uk/spm/, last accessed August 30, 2014). Preprocessing steps included slice timing correction, realignment, spatial coregistration, normalization, and smoothing. Specifically, slice timing correction was carried out using sinc interpolation to correct for differences in slice acquisition time within an EPI volume. The images were then spatially realigned to the first image of each session by a 6-parameter rigid body spatial transformation to account for head movement during acquisition. Each subject's images were then normalized and registered to the Montreal Neurological Institute (MNI) space. All images were further resampled to a voxel size of 3 × 3 × 3 mm, and spatially smoothed using a Gaussian kernel with 8 mm full width at half maximum. Slow temporal drifts in baseline were removed by applying a high-pass filter with cutoff frequency set at 1/128 Hz. Global effects were accounted for by using the proportional scaling approach which divides the signal from each voxel by the spatial average of signals from all cerebral voxels (Fox et al. 2009).

EEG Spectral Analysis

EEG power spectral density (PSD) was calculated on the CSD data in the period from 500 to 1000 ms after cue onset (Fig. 2*A*) using the FFT-based periodogram approach. To calculate the grand average power spectrum across subjects, the power spectrum from each subject was normalized by dividing the PSD by that subject's mean alpha power from the attend-left condition. Such normalization was not performed when correlating alpha power with the BOLD signal. For each subject, trial-by-trial spectral power in the alpha band was calculated by integrating the unnormalized single-trial power spectrum within the range of 8–12 Hz in regions of interests (ROIs) over occipito-parietal sites where alpha showed the strongest attentional effects (Fig. 2*B,C*; left hemisphere: O1 and P3; right hemisphere: O2 and P8). The selected posterior scalp ROIs for EEG alpha analysis corresponded well to the scalp regions used in previous studies (e.g., Worden et al. 2000; Thut et al. 2006). For trials rejected during preprocessing because of EEG artifacts, we used the mean alpha power calculated within the same condition as substitutes, to allow for regression with trial-by-trial BOLD activity in subsequent EEG-informed fMRI analysis.

To measure alpha asymmetry, a single-trial alpha hemispheric lateralization index was defined as (Thut et al. 2006):

$$\text{Index}\,(\alpha) = \frac{\alpha_{\text{ipsilateral ROI}} - \alpha_{\text{contralateral ROI}}}{\text{mean}(\alpha_{\text{ROIs from both condition}})}.$$

The above lateralization index measures the percentage difference between single-trial alpha amplitudes from ROIs ipsilateral and contralateral to the attended visual field. Larger values of the above index indicate stronger lateralization of alpha due to attention.

FMRI Activation Analysis

The BOLD responses were examined using general linear models (GLMs) as implemented in SPM5. In total, 8 task-related regressors were included in the GLM to model the following stimulus events: 2 regressors separately modeled BOLD activity related to leftward and rightward cues with correct responses; 2 additional regressors modeled BOLD responses evoked by target stimuli appearing on the left and right visual fields; a fifth regressor of no interest was added to model cue events with incorrect responses; finally, the choice cues as well as the side-reporting were also included in the GLM as regressors of no interest to account for BOLD activity evoked by these events. Group-level cue-evoked fMRI activations were obtained by a parametric one-sample *t*-test and were considered statistically significant at $P < 0.05$, corrected for multiple comparisons by controlling the false discovery rate (FDR).

Event-related BOLD responses to target stimuli in the visual cortex were estimated via a GLM with finite impulse response (FIR) model as implemented in MarsBaR region of interest toolbox (http://marsbar.sourceforge.net/, last accessed August 30, 2014). Activations in visual cortex by targets were identified by examining the positive BOLD activations by target stimuli under $P < 0.05$, FDR (Fig. 2*E*). A 3-mm-radius spherical ROI was then seeded around the peak voxel in the left and right calcarine sulci to estimate evoked BOLD activities via the above FIR model. Attentional enhancement related to target processing in the above calcarine ROIs were assessed via a 3-way analysis of variance (ANOVA) with repeated measures on the peak BOLD responses with Target Cueing (cued vs. uncued), Target Hemifield (left vs. right), and Hemisphere (left ROI vs. right ROI) as factors.

EEG-informed fMRI Analysis

In addition to the above task-related regressors, coupling effects between alpha oscillations and BOLD were modeled in the GLM using parametric modulations based on single-trial alpha power. Specifically, 3 separate GLMs were constructed to model 3 aspects of coupling between BOLD and EEG alpha rhythm: (1) coupling between BOLD and alpha power measured in ROIs contralateral to the attended hemifield, (2) between BOLD and alpha power measured in ROIs ipsilateral to the attended hemifield, and (3) between BOLD and attention-induced alpha lateralization. For the first 2 GLMs (Models 1 and 2), 2 regressors modeling attentional modulation of alpha power were included in the design matrix with onsets of the boxcar functions specified according to cue onset timings in attend-left and attend-right conditions. The height of each boxcar function modeling each trial within these regressors was multiplied by the single-trial alpha power sampled from the contralateral ROI in Model 1 and from the ipsilateral ROI in Model 2. To orthogonalize the parametric modulation with respect to regressors modeling cue-related activities, the mean alpha power across trials within a session was subtracted from single-trial alpha powers for the corresponding cue conditions. The resultant regression coefficients indicate the strength of coupling between BOLD and alpha power measured separately on the contralateral and ipsilateral ROIs. In the third model (Model 3), the interaction between BOLD and the degree of alpha hemispheric lateralization was modeled by a set of parametric modulations derived from the single-trial alpha lateralization index. Specifically, in Model 3, 2 new regressors were included in the GLM in the same way as in Models 1 and 2 for the attend-left and attend-right conditions, but with the height of the boxcar

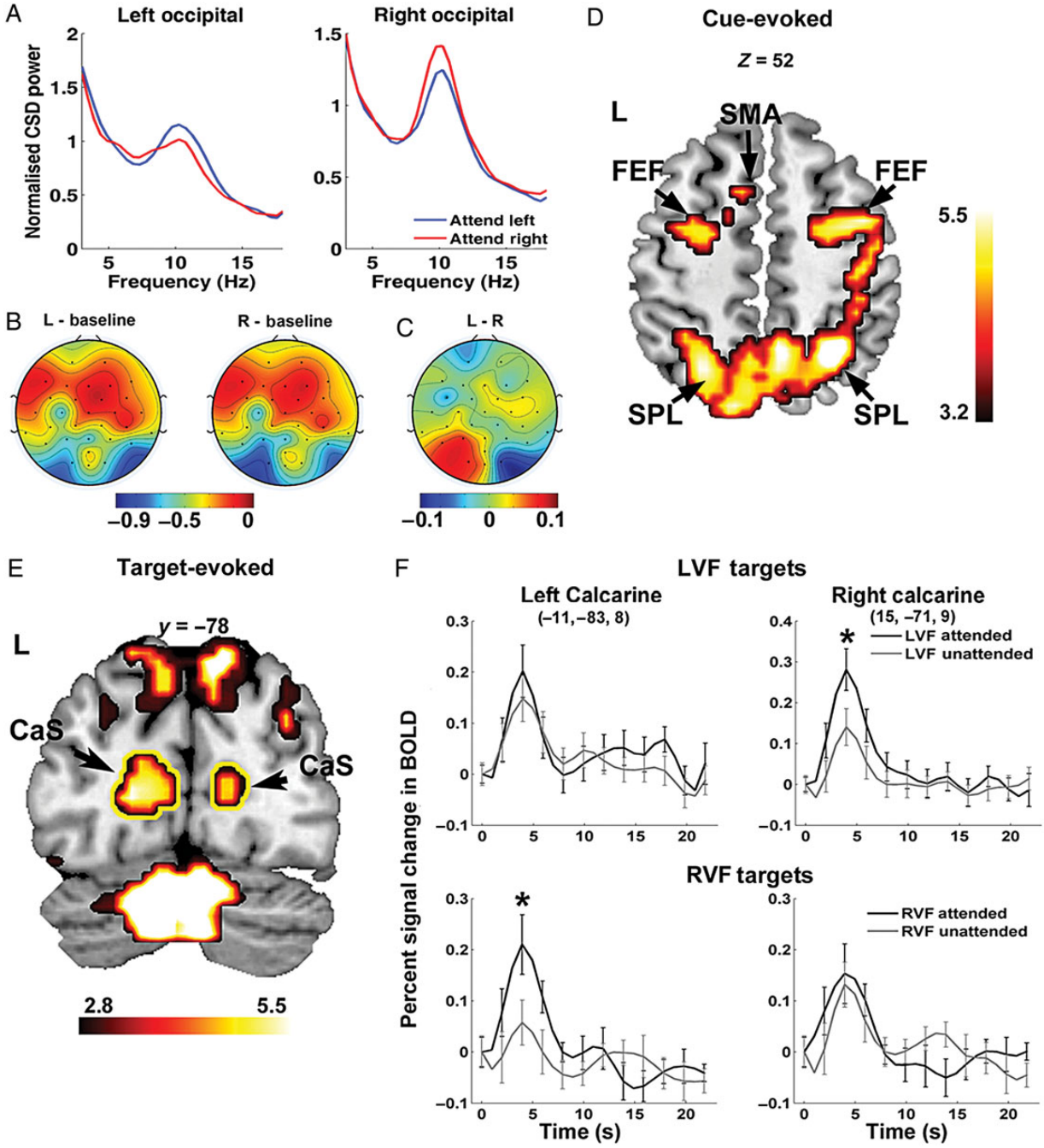

Figure 2. Attentional modulation of alpha power and BOLD activations. (*A*) Grand average power spectral density from occipital channels (O1 and O2) showing attentional modulation of alpha (8–12 Hz) during 500–1000 ms after cue onset. (*B*) Scalp topography showing alpha percentage desynchronization relative to the precue baseline during attend-left (L) and attend-right (R) conditions, respectively. (*C*) Difference topography contrasting attend-left and attend-right conditions showing asymmetry in alpha desynchronization. Color bars in (*B*) and (*C*) reflect percentage changes in alpha power. (*D*) BOLD activations evoked by the cue showing the engagement of the dorsal attention network during the postcue anticipatory period. (*E*) A coronal slice ($y = -78$) showing target-evoked activities in the calcarine sulcus (outlined in yellow), parietal cortices, and the cerebellum. (*F*) Enhanced BOLD activity ($P < 0.05$) for attended relative to unattended targets in the calcarine sulcus contralateral to the target location. Activation maps are thresholded at $P < 0.05$, FDR corrected, and plotted according to the neurological convention with left shown on the left side. FEF: frontal eye field; IPS: intraparietal sulcus; SPL: superior parietal lobule; SMA: supplementary motor area; CaS: calcarine sulcus; LVF: left visual field; RVF: right visual field.

functions modeling each cue onset multiplied by the mean-removed single-trial alpha lateralization index. All task-relevant regressors were convolved with a canonical hemodynamic response function to allow for comparisons with the recorded BOLD signal. Six movement-related regressors were further incorporated into the design matrix to regress out residual signal variance from head movement.

At the individual subject level, the coupling between BOLD and alpha modulation was assessed by examining, via *t*-contrasts, the significance of the coefficients related to the alpha regressors. At the group level, systematic alpha-BOLD coupling was further assessed via a second-level random effects analysis using the contrast images from individual-level alpha-BOLD coupling analysis via a nonparametric permutation testing scheme as implemented in SnPM (Statistical Nonparametric Mapping, http://go.warwick.ac.uk/tenichols/snpm, last accessed August 30, 2014). Compared with the parametric tests, nonparametric permutation tests require much weaker assumptions

about properties of data samples (Nichols and Holmes 2001) and hence, are more suitable for EEG data recorded concurrently with fMRI where multiple sources of noise/uncertainty in the EEG-related regressors might render the normality assumption untenable. The test first shuffles the condition labels of each sample in the group and computes the test statistic for each relabeling to construct an empirical distribution of the test statistic under the null hypothesis. Then, the actual observed test statistic was compared against the critical value derived from the empirical distribution to assess statistical significance.

EEG-BOLD couplings are typically weak because they measure the residual effects after the mean evoked BOLD responses are removed. Past work using voxel-wise thresholds of $P < 0.001$ or $P < 0.005$, uncorrected, has yielded highly interpretable statistical brain maps (Laufs et al. 2003; Debener et al. 2005; Eichele et al. 2005; Liu et al. 2012). Here, additional requirements that the coupling should be consistently observed across all individual subjects and the activated cluster contains at least 5 voxels were adopted. To further test the statistical robustness of activated regions, we utilized the maximal statistic approach as discussed in Nichols and Holmes (2001) to correct for multiple comparisons and limit family-wise Type I errors. Specifically, the family-wise Type I error was controlled by thresholding the observed statistical map using a cluster-level critical value derived from the permutation distribution of the *maximal suprathreshold cluster size* from every possible relabeling (Holmes et al. 1996). The primary threshold used in this study to generate suprathreshold clusters was $P < 0.005$, uncorrected. Alpha-BOLD coupling effects exceeding the 95th percentile of the above permutation distribution of the maximal suprathreshold cluster size were denoted $P_{FWE} < 0.05$ under this correction scheme. It has been suggested that this type of cluster-level threshold is more suitable for multiple comparison correction in fMRI data than typical single-voxel based approaches such as the FDR implemented in SPM (Nichols and Holmes 2001).

Results

For the 13 subjects included in the analysis, the mean accuracy rates for discriminating the spatial frequency of the grating stimuli were 85.4% for attend-left and 86.0% for attend-right conditions, respectively. No difference was observed in reaction time between attend-left (mean = 927.94 ms; SD = 101.16 ms) and attend-right (mean = 911.38 ms; SD = 82.92 ms) conditions (paired *t*-test, $P = 0.38$).

Attention-related Modulation of Occipital Alpha

The average alpha peak frequency was 10.2 Hz with a standard deviation of 0.94 Hz among the 13 subjects. For the chosen postcue/pretarget analysis window (500–1000 ms postcue), posterior alpha over both hemispheres was lower than a precue baseline defined to be 500 ms before cue onset (Fig. 2*B*), with a stronger decrease in alpha power over the occipital scalp region contralateral to the attended hemifield (Fig. 2*A*; left hemisphere: $t_{12} = -2.1462$, $P < 0.05$; right hemisphere: $t_{12} = -1.9145$, $P < 0.05$). Topographically, the difference in the degree of alpha suppression between 2 hemispheres gave rise to the hemispheric lateralization pattern seen in Figure 2*C*, in which alpha power from the attend-right condition was subtracted from the attend-left condition. This lateralization pattern in posterior alpha matches findings reported in prior studies of visual spatial attention (e.g., Worden et al. 2000; Thut et al. 2006).

Attentional Control: BOLD Activations Evoked by the cue

Significant BOLD activations in areas within the dorsal attention network were observed in the postcue interval, including bilateral FEF, IPS, and regions within the superior parietal lobule (Fig. 2*D*). This activation pattern is in line with those typically observed in the attention literature (e.g., Corbetta and Shulman 2011), and in conjunction with the postcue lateralization of alpha, indicates that participants properly allocated their covert attention during the cue-to-target interval according to cue instructions. Other regions activated during the anticipatory period included the supplementary motor area (SMA), precuneus, ventral occipitotemporal cortex, and middle temporal complex (MT+). The coordinates of all the activated regions are listed in Table 1.

Table 1
Regions showing event-related BOLD activations following cue onset

Anatomical regions	Hemisphere	MNI coordinates (*x*, *y*, *z*)	*Z*-score
Frontal eye field	Left	−24, −3, 57	3.56
	Right	39, 0, 57	4.15
Intraparietal sulcus	Left	−33, −48, 42	4.10
	Right	27, −57, 51	5.13
MT+	Left	−48, −69, −15	5.25
	Right	51, −72, −12	5.24
Ventral occipitotemporal cortex	Left	−51, −64, −20	4.84
	Right	51, −70, −11	4.63
Precuneus	Left	−6, −57, 57	3.78
	Right	6, −54, 54	3.98
Supplementary motor area	Left	−9, 12, 51	3.16

Attentional Selection of Sensory Signals: BOLD Activations Evoked by the Target

Target stimuli evoked significant BOLD activations in the visual cortex within the calcarine sulcus and adjacent lingual gyrus (Fig. 2*E*, outlined in yellow; MNI coordinates for left calcarine: −11, −83, 8; right calcarine: 15, −71, 9). To assess whether spatial attention enhances target processing in the visual cortex, event-related BOLD responses in ROIs within the calcarine cortex were extracted for attended and unattended targets in the left and right hemifield (Fig. 2*F*). Enhanced BOLD activity was observed in calcarine ROIs contralateral to the attended target location. We conducted a 3-way repeated-measures ANOVA with Target Cueing (cued vs. uncued), Target Hemifield (left vs. right), and Hemisphere (left ROI vs. right ROI) as within-subject factors and identified a significant main effect of Target Cueing ($F_{1,12} = 6.171$, $P < 0.05$), and a significant 3-way interaction among Target Cueing, Target Hemifield, and Hemisphere ($F_{1,12} = 6.366$, $P < 0.05$). Follow-up analyses via paired *t*-tests on peak BOLD responses confirmed that for left visual field targets, significant attentional enhancement toward target stimuli (cued > uncued) was observed only in the right visual cortex (RH: $P < 0.05$, corrected; LH: n.s.), while for right visual field targets, attentional enhancement was only observed in the left visual cortex (LH: $P < 0.01$, corrected; RH: n.s.). The increased amplitude of BOLD response for attended targets in the visual cortex is consistent with prior fMRI studies of spatial attention (e.g., Hopfinger et al. 2000), and provides additional evidence that the subjects oriented spatial attention according to the cues.

BOLD-alpha Coupling: Inverse Correlations

Combining attend-left and attend-right conditions, the alpha contralateral to the cued hemifield was inversely correlated with BOLD in bilateral IPS, left middle frontal gyrus, left ventral occipital cortex (VO), right inferior and middle temporal gyrus (IT/MTG), and left cerebellum (crus I and II), at $P < 0.001$, uncorrected (Fig. 3*A*, first row). That is, on a

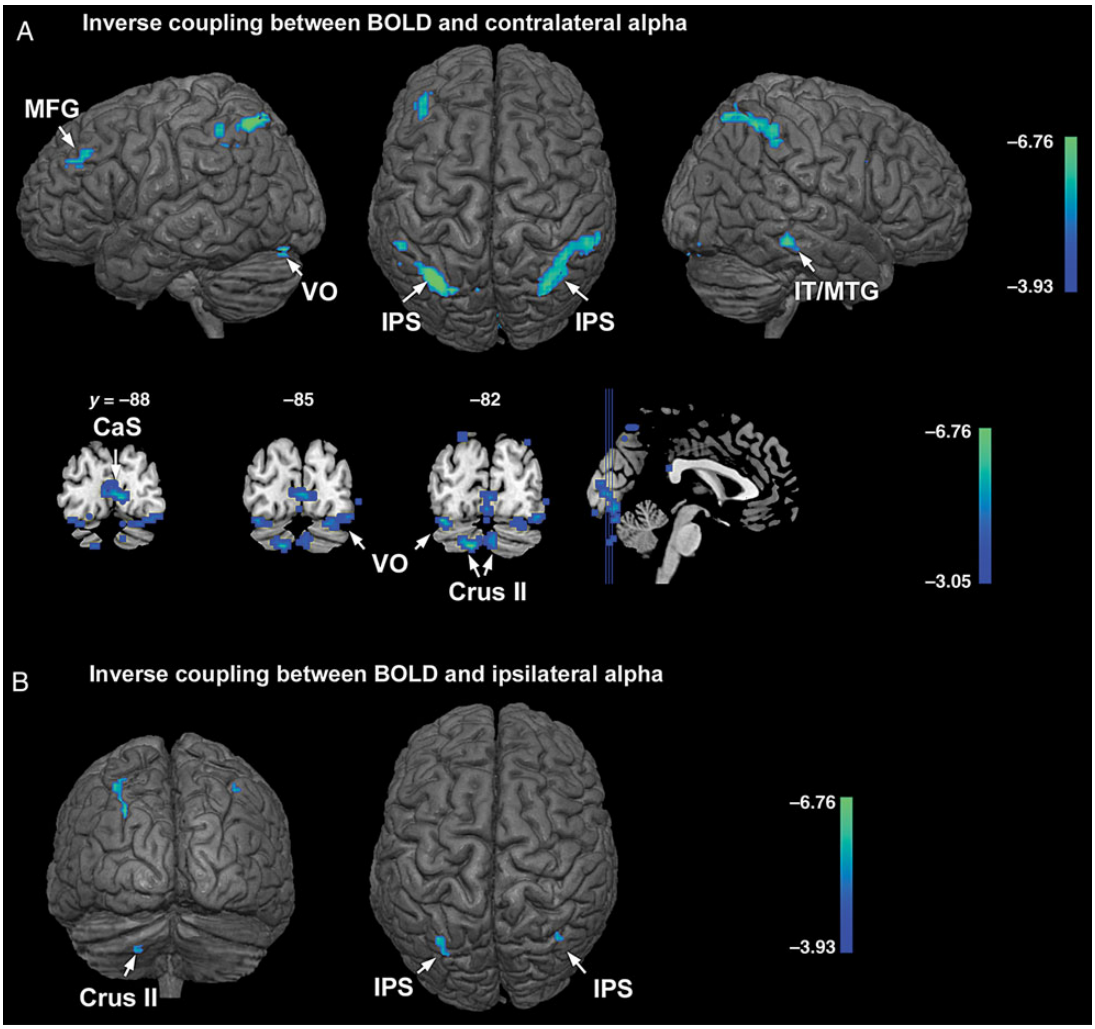

Figure 3. Regions showing inverse coupling between BOLD and alpha with attend-left and attend-right conditions combined. (*A*) Regions showing inverse coupling with contralateral alpha during anticipatory attention (first row and second row were thresholded at $P < 0.001$ and $P < 0.005$, uncorrected, respectively). (*B*) Regions showing inverse coupling between BOLD and ipsilateral alpha ($P < 0.001$, uncorrected). IPS: intraparietal sulcus; MFG: middle frontal gyrus; IT: inferotemporal gyrus; MTG: middle temporal gyrus; VO: ventral occipital cortex; CaS: calcarine sulcus; crus II: crus II of cerebellum.

trial-by-trial basis, when these brain regions were more active, alpha was more reduced over the occipital scalp contralateral to the cued hemifield. Among the above regions, bilateral IPS and the left cerebellum showed stronger inverse coupling with contralateral alpha at $P_{FWE} < 0.05$ (cluster-level threshold; left IPS: 222 voxels; right IPS: 262 voxels; left cerebellum: 55 voxels). Under a voxel-level statistical threshold of $P < 0.005$, uncorrected, BOLD signals from extended regions in the calcarine sulcus (CaS), bilateral VO, and bilateral crus II regions of the cerebellum further showed inverse correlations with alpha power in the hemisphere contralateral to the cued hemifield (Fig. 3*A*, second row). For alpha ipsilateral to the cued hemifield, regions showing inverse BOLD-alpha correlations at $P < 0.001$, uncorrected, included bilateral IPS and crus II of the left cerebellum (Fig. 3*B*; Table 2). These correlations were generally weaker as no region showed a coupling strength that reached $P_{FWE} < 0.05$. The coordinates of the regions showing inverse alpha-BOLD coupling are listed in Table 2.

A ROI-based analysis within the IPS revealed that the mean number of voxels showing significant inverse BOLD-alpha coupling in the left and right IPS clusters were 184 and 55, respectively, for ipsilateral alpha, while for contralateral alpha the respective cluster sizes were 222 and 262; the contralateral alpha-BOLD coupling cluster sizes were significantly larger than for the ipsilateral alpha-BOLD coupling ($P < 0.001$, one-sided, paired *t*-test; test performed on 500 bootstrap samples constructed by resampling the subjects with replacement; Fig. 4*A*). In addition to differences in cluster size, the inverse coupling strength between alpha and the left IPS, measured by the coefficient in front of the regressor representing contralateral or ipsilateral alpha collapsed across attend-right and attend-left conditions, was stronger (more negative) for contralateral alpha than ipsilateral alpha (coupling strength for contralateral alpha: −1.26; ipsilateral alpha: −0.96; $P < 0.05$, one-sided, paired *t*-test; Fig. 4*B*). Yet, in right IPS, the inverse coupling was only marginally stronger for contralateral alpha compared with ipsilateral alpha (coupling strength for contralateral alpha: −1.04; ipsilateral alpha: −0.96; n.s.; Fig. 4*B*). These results suggest that the coupling between IPS and the ipsilateral alpha is generally weaker than that for contralateral alpha. It is worth noting that no coupling (positive or inverse) was observed between alpha and BOLD signals in the FEF.

BOLD-alpha Coupling: Positive Correlations

For alpha recorded from the occipital scalp contralateral to the cued hemifield, areas showing positive BOLD-alpha correlation included regions within the precentral gyrus (pre-CG), postcentral gyrus (post-CG), and middle temporal gyrus (MTG), at $P < 0.001$, uncorrected (Fig. 5*A*). That is, on a trial-by-trial basis, these brain regions showed decreased BOLD activity when alpha power also decreased. Among these regions, the positive coupling between bilateral post-CG and contralateral alpha is stronger, reaching $P_{FWE} < 0.05$ (cluster-level threshold; left post-CG: 64 voxels; right post-CG: 47 voxels). For ipsilateral alpha, BOLD in medial prefrontal cortex (MPFC) and adjacent cortices in the superior frontal gyrus (SFG) showed positive correlation at $P < 0.001$, uncorrected (Fig. 5*B*). No region showed significant positive coupling with ipsilateral alpha under $P_{FWE} < 0.05$. While pre- and post-CG are in the sensorimotor cortices, the MPFC and MTG are core nodes of the default mode network (DMN). Table 2 lists the coordinates of regions that show positive correlations with alpha.

Table 2
Coupling between alpha and BOLD with attend-left and attend-right combined[a]

Anatomical regions	Hemisphere	MNI coordinates (*x*, *y*, *z*)	*t*-value
Inverse coupling between BOLD and contralateral alpha			
Intraparietal sulcus	Left	−33, −63, 57	8.73*(222)
	Right	39, −51, 54	6.98*(262)
Inferior and middle temporal gyrus	Right	60, −33, −15	6.58
Middle frontal gyrus	Left	−39, 42, 33	5.24
Ventral occipital cortex	Left	−35, −81, −17	6.48
	Right	42, −84, −15	4.24
Calcarine sulcus		9, −87, 0	5.11
Crus I of cerebellum	Left	−30, −72, −33	8.05*
Crus II of cerebellum	Left	−12, −81, −39	7.04*(55)
	Right	3, −81, −33	3.55**
Inverse coupling between BOLD and ipsilateral alpha			
Intraparietal Sulcus	Left	−30, −63, 39	6.02
	Right	36, −63, 51	4.59
Crus II of Cerebellum	Left	−21, −75, −42	4.55
Positive coupling between BOLD and contralateral alpha			
Postcentral gyrus	Left	−48, −12, 24	7.86*(64)
	Right	60, −12, 39	7.49*(47)
Precentral gyrus	Left	−12, −15, 63	5.62
Middle temporal gyrus	Left	−57, −9, −18	5.15
Positive coupling between BOLD and ipsilateral alpha			
Medial prefrontal cortex	Right	15, 48, 33	7.45
Positive coupling between BOLD and alpha lateralization index			
Dorsal anterior cingulate cortex	Right	6, 24, 39	4.66
Medial prefrontal cortex	Right	15, 51, 27	5.77
Superior frontal gyrus	Left	−21, 36, 39	5.19

[a]Regions included were thresholded by default at $P < 0.001$, uncorrected, if not stated otherwise.
*$P_{FWE} < 0.05$, corrected for multiple comparisons using a cluster-level nonparametric permutation test. Cluster sizes under the primary threshold of $P < 0.005$, uncorrected, are reported in parentheses. Note the crus I and crus II of the left cerebellum form one connected cluster and the combined cluster size is reported.
**$P < 0.005$, uncorrected.

Coupling Between Alpha Lateralization Index and BOLD

The analysis in the foregoing 2 sections focused on the alpha power recorded over either the occipital hemispheres contralateral or ipsilateral to the cued hemifield. The degree of alpha lateralization, defined as ipsilateral alpha minus contralateral alpha normalized by their sum, assesses the alpha difference between the 2 hemispheres and is an important indicator of attentional control, with greater alpha lateralization signifying a more efficient allocation of spatial attention (Thut et al. 2006; Haegens et al. 2011; Händel et al. 2011). Correlating the trial-by-trial alpha lateralization index with BOLD activity, we found positive correlation between the alpha lateralization index and BOLD activity in regions within the dACC, as well as adjacent areas of right MPFC and left dorsal lateral prefrontal cortex (DLPFC) (superior frontal gyrus, SFG, Brodmann area 9) (Fig. 6*A,B*; Table 2). That is, on a trial-by-trial basis, when alpha was more strongly lateralized, BOLD signals in these regions were of greater amplitude. ROI-based analysis within the dACC showed that the strength of positive coupling, measured by the coefficient in front of the regressor representing alpha lateralization collapsed across attend-right and attend-left conditions, was highly consistent across participants (positive coupling observed in 12 out of 13 participants with the only exception of Subject 9; Fig. 6*C,D*), suggesting that the observed effect was not likely to be caused by outliers. These regions, especially dACC, have been hypothesized to be part of a "core" or "task control" or "salience" network responsible for maintaining executive control over the ongoing task (Dosenbach et al. 2008). No regions were found to be inversely correlated with the alpha lateralization index.

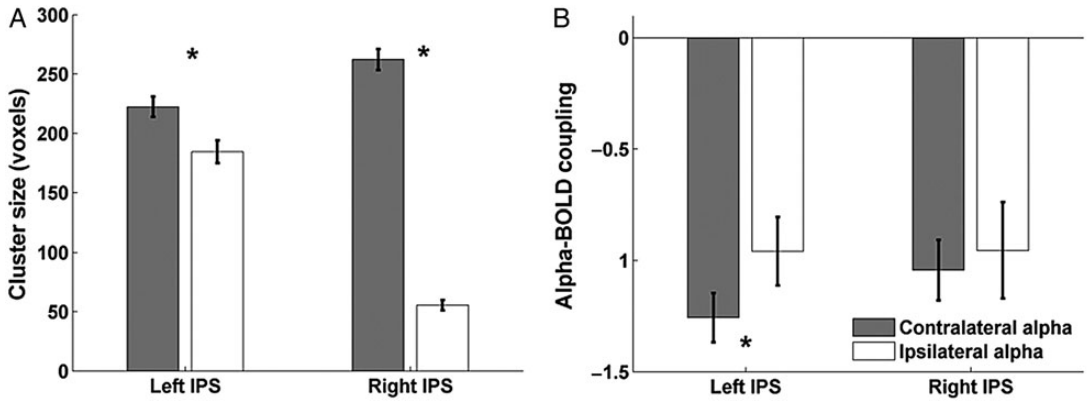

Figure 4. Coupling between BOLD and alpha within the IPS. (*A*) Cluster sizes in left and right IPS showing significant inverse coupling with contra- and ipsilateral alpha collapsed across attend-left and attend-right conditions. The mean and standard error in cluster size were obtained by bootstrapping 500 times on the group level. (*B*) Coupling strength between BOLD and alpha within the IPS clusters for contralateral and ipsilateral alpha, respectively. A significantly stronger inverse coupling was observed in left IPS for contralateral alpha compared with ipsilateral alpha. Error bars represent standard error of mean on the group level. Here the coupling strength is measured by the coefficient in front of the regressor representing contralateral or ipsilateral alpha power collapsed across attend-right and attend-left conditions.

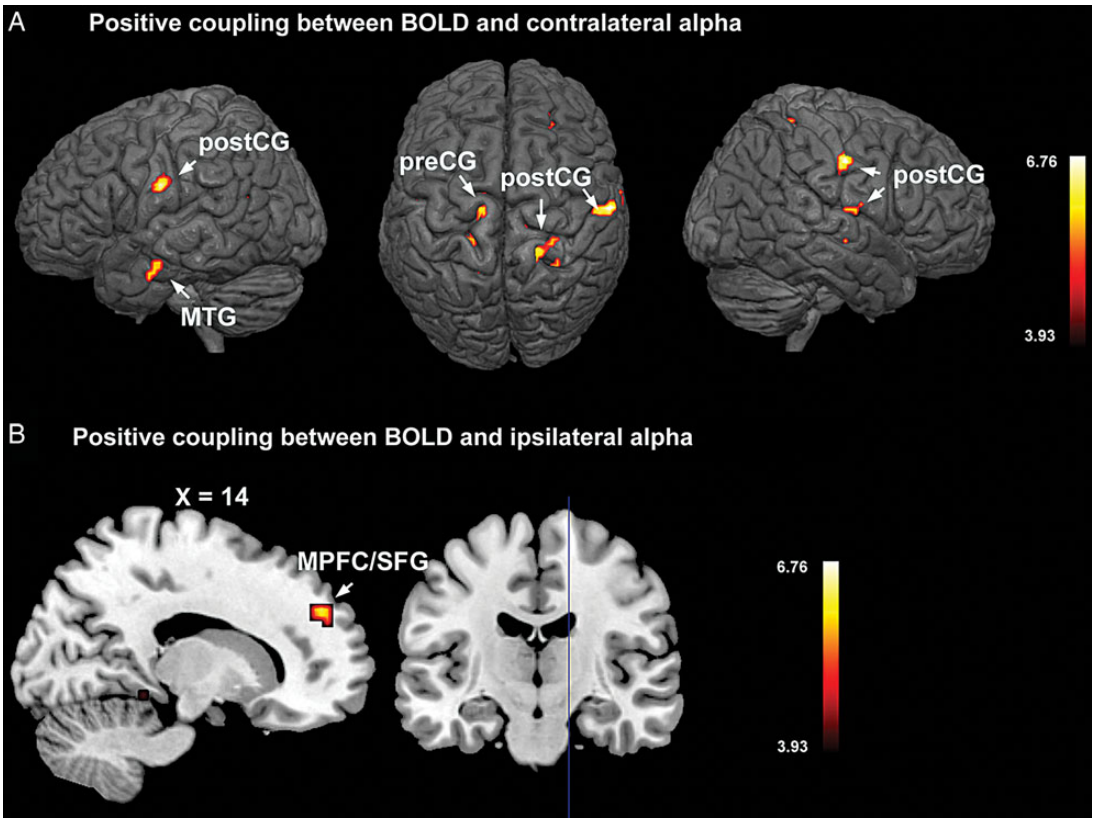

Figure 5. Regions showing positive coupling between BOLD and alpha with attend-left and attend-right combined. (*A*) Regions showing positive BOLD coupling with contralateral alpha. (*B*) Regions showing positive coupling with ipsilateral alpha. The statistical parametric maps are thresholded at $P < 0.001$, uncorrected. MPFC: medial prefrontal cortex; MTG: middle temporal gyrus; post-CG: postcentral gyrus; SFG: superior frontal gyrus.

Discussion

Top-down, anticipatory control of spatial attention enhances the processing of attended stimuli by biasing sensory cortex before stimulus onset. The lateralization of alpha oscillations is a manifestation of this biasing action in visual (Worden et al. 2000; Sauseng et al. 2005; Thut et al. 2006) and somatosensory domains (Anderson and Ding 2011; Haegens et al. 2011). The present work examined brain structures that contribute to the modulation of visual alpha oscillations during anticipatory attention by recording simultaneous EEG-fMRI from human subjects performing a cued visual spatial attention task. Unlike prior resting-state fMRI studies reporting BOLD correlates of alpha oscillations in the frontoparietal network (Laufs et al. 2003), the current study directly addresses the mechanism of top-down attentional modulation by examining functional links between BOLD and alpha under an active state of covert spatial attention. Correlating hemispheric alpha power and cross-hemisphere alpha lateralization with concurrently recorded BOLD signals, we found that: (1) alpha decreases contralateral to the cued hemifield were associated with BOLD increases in IPS, as well as in visual areas; (2) decreases in alpha contralateral to the cued hemifield were also associated with BOLD decreases in the sensorimotor cortices and the default mode network; and (3) the degree of alpha lateralization was positively coupled with BOLD in dACC/MPFC and regions of DLPFC.

Alpha and Dorsal Attention Network

One putative source of attentional modulation of alpha is the dorsal attention network, which is hypothesized to generate and maintain a top-down expectation signal to selectively bias visual cortical activity (Gitelman et al. 1999; Hopfinger et al. 2000; Corbetta and Shulman 2002). Here, we provide evidence that increased BOLD in bilateral IPS is most strongly coupled with desynchronized EEG alpha in the hemisphere contralateral to the direction of spatial attention during anticipatory attention. Our results are consistent with 2 recent studies employing rTMS showing disrupted posterior alpha desynchronization following interference of preparatory activities in the IPS (Capotosto et al. 2009, 2012).

Whether successful attention allocation is primarily achieved by an enhancement of task-relevant visual cortices, a suppression of task-irrelevant areas, or a combination of the 2 processes, is still debated. Evidence in terms of anticipatory alpha is also mixed. Some studies attribute selective attention to a mechanism of decreased alpha contralateral to the attended location (Sauseng et al. 2005; Thut et al. 2006; Grent-'t-Jong et al. 2011), whereas other studies suggest that visuospatial attention functions by inhibiting the hemisphere contralateral to the unattended hemifield (Foxe et al. 1998; Worden et al. 2000; Yamagishi et al. 2003; Kelly et al. 2006; Händel et al. 2011). It should be noted that only a few studies were able to observe a net increase in alpha power relative to baseline over the hemisphere contralateral to the unattended location (Yamagishi et al. 2003; Kelly et al. 2006). In the current study, we observed alpha decreases in both hemispheres with respect to the baseline, with stronger a decrease in the hemisphere contralateral to the attended location (Rajagovindan and Ding 2011). The stronger inverse coupling between

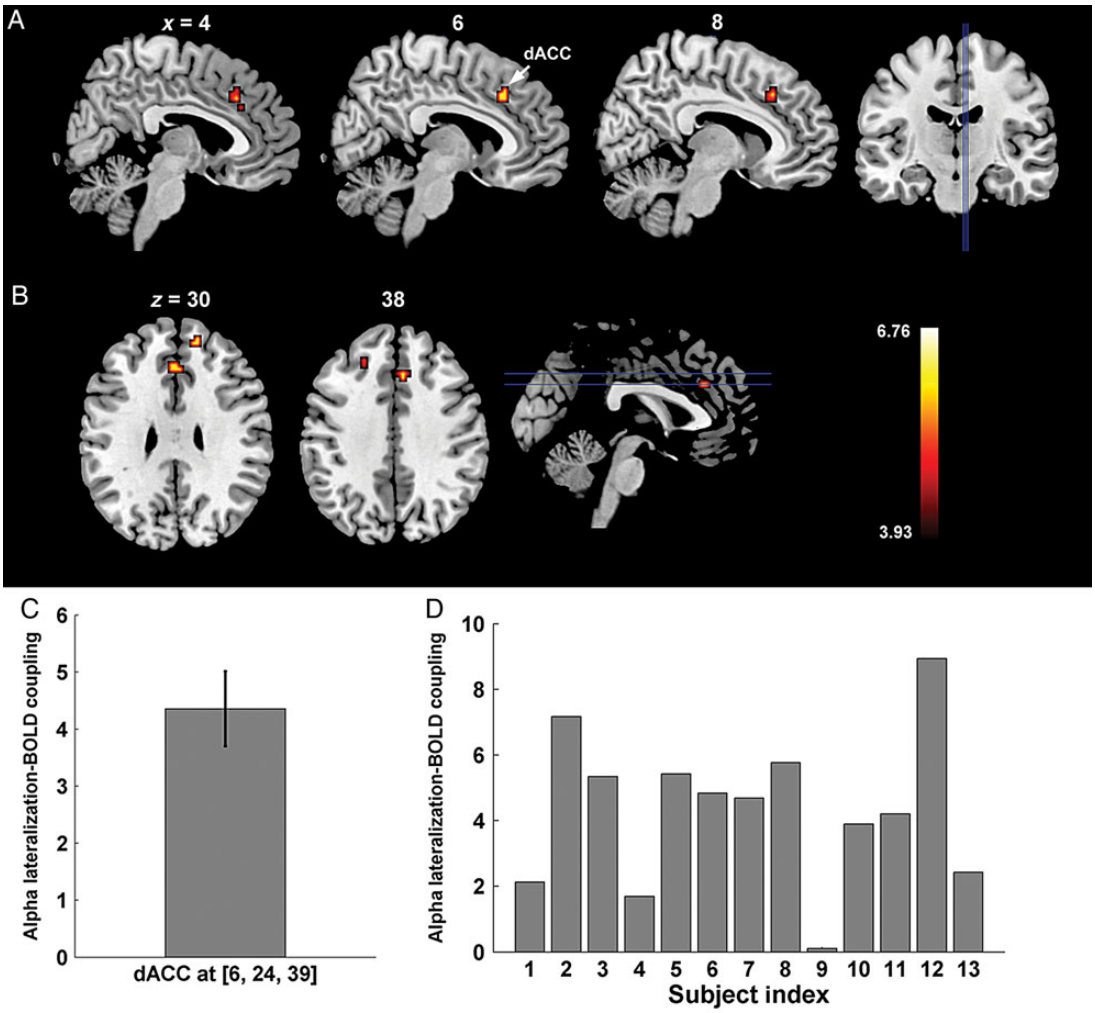

Figure 6. Regions showing coupling between BOLD and alpha lateralization index. (*A*) Sagittal slices showing a region in dorsal anterior cingulate cortex (dACC) whose BOLD is positively correlated with alpha lateralization. (*B*) Coronal slices showing the same region in dACC, along with adjacent regions in the medial prefrontal cortex (MPFC) and superior frontal gyrus (SFG; Brodmann Area 9), a component of the dorsal lateral prefrontal cortex (DLPFC). (*C*) Coupling strength between BOLD and alpha lateralization index within dACC averaged within the activated cluster around (6, 24, 39). (*D*) Individual-level coupling strengths showing consistent positive coupling across subjects between BOLD and alpha lateralization within the same dACC region shown in C). Here the coupling strength is measured by the coefficient in front of the regressor representing alpha lateralization collapsed across attend-right and attend-left conditions.

contralateral alpha and BOLD in IPS, compared with ipsilateral alpha, appears to suggest that the IPS operates mainly by enhancing neuronal activity within task-relevant visual cortical areas (Corbetta and Shulman 2002). Alpha increases over areas ipsilateral to the attended locations are often observed in tasks demanding active suppression of distractors at unattended locations (Yamagishi et al. 2003; Kelly et al. 2006). This is not a strong requirement in our task and likely resulted in our findings being clearest for the contralateral alpha.

Alpha and Task-irrelevant Networks

Posterior alpha in the current study was found to be positively correlated with BOLD in sensorimotor cortices, as well as regions within the default mode network (DMN). This indicates that elevated visual cortical excitability, as indicated by decreased posterior alpha, is accompanied by decreased activity within task-irrelevant cortices in other sensory or cognitive modalities. Such a "push-pull" mechanism has been observed in past studies involving attention to multiple sensory modalities (Klimesch et al. 2007; Jensen and Mazaheri 2010). For example, visual alpha is found to be increased when attention is directed to the somatosensory (Haegens et al. 2010; Anderson and Ding 2011) or the auditory domains (Foxe et al. 1998; Fu et al. 2001). Similarly, higher levels of alpha activity within visual cortices were associated with enhanced performance toward auditory stimuli (Bollimunta et al. 2008). The current study extends this mechanism to include the DMN, which is known to mediate non-sensory self-referential processes (Buckner et al. 2008). Interestingly, it has been demonstrated that even under resting-state, when external task performance is minimal, positive coupling between spontaneous visual alpha fluctuations and BOLD in the DMN occurs, demonstrating an intrinsic dynamic interaction between different cortical systems (Mayhew et al. 2013; Mo et al. 2013). In light of this, visual attention might modulate such intrinsic functional interactions to selectively inhibit task-irrelevant networks to facilitate processing in the ongoing visual task. It is worth noting that the ipsilateral alpha was only coupled with nodes in DMN, whereas the contralateral alpha showed coupling with both DMN and the sensorimotor network. The additional coupling

within the sensorimotor network for contralateral alpha further suggests that the "push-pull" mechanism is more active over the hemisphere contralateral to the attended location.

Differential Roles of IPS and FEF in Controlling Alpha

A somewhat surprising finding was that alpha power was not coupled with BOLD in FEF, suggesting differential roles of FEF and IPS in modulating visual alpha during anticipatory spatial attention. This finding is consistent with a recent dynamic causal modeling study showing direct modulation of the visual cortex by IPS instead of FEF (Vossel et al. 2012). Further, rTMS on IPS, but not FEF, has been shown to induce a paradoxical increase in alpha during anticipatory attention (Capotosto et al. 2009). Taken together, the coupling between IPS and visual alpha found in our study suggests that IPS, instead of FEF, directly modulates the visual cortical excitability reflected in alpha power. Although a host of studies have reported involvement of FEF in modulating visual cortex during attention (Ruff et al. 2006, 2008; Bressler et al. 2008; Capotosto et al. 2009; Armstrong et al. 2012), it is possible that such involvement reflects an indirect engagement of FEF in modulating visual cortices, through changes in inter-regional EEG synchrony rather than regional alpha desynchronization (Sauseng et al. 2005, 2011).

The Role of Frontal Executive Areas in Controlling Alpha Lateralization

Past studies have proposed that the allocation of attentional resources during spatial attention is reflected in the degree of lateralization of alpha across 2 hemispheres (Thut et al. 2006; Händel et al. 2011). In line with this, it has been shown that stronger alpha lateralization is associated with shorter reaction times (Thut et al. 2006; Kelly et al. 2009; Haegens et al. 2011). Our findings that the degree of alpha lateralization is positively coupled with BOLD activity in dACC and adjacent prefrontal areas, including the right MPFC and the left DLPFC, are consistent with the known function of these frontal executive areas. Activated in a variety of cognitive tasks, dACC is considered part of a task control or salience network engaged in maintaining a global task-set to mediate goal-directed behavior (Dosenbach et al. 2006, 2008; Sakai 2008). This network, containing dACC and bilateral anterior insula, is hypothesized to issue top-down signals to other domain-specific executive areas to ensure the proper allocation of resources to support various task-specific activities (Shulman et al. 2003; Crottaz-Herbette and Menon 2006; Dosenbach et al. 2006; Aarts et al. 2008; Walsh et al. 2011; Wen et al. 2013). Similarly, DLPFC, reciprocally connected with dACC (Selemon and Goldman-Rakic 1988), is known to be critical in the maintenance of task rules and implementation of cognitive control (MacDonald et al. 2000; Dosenbach et al. 2008). By demonstrating that both structures are involved in the regulation of sensory cortical activity as indexed by attention-related alpha lateralization, the current study sheds lights on the roles of these frontal executive areas in visual spatial attention, which to date has remained unclear.

It should be noted that the positive coupling between dACC/DLPFC and alpha lateralization is relatively weak, and did not reach the threshold of $P_{FWE} < 0.05$ based on the whole-brain correction for multiple comparisons. This weak coupling strength might be caused by the low signal-to-noise ratio in the single-trial alpha lateralization index, or it could suggest an overall weak coupling between these frontal executive structures and alpha lateralization, which may implicate an indirect role of dACC/DLPFC in modulating alpha. Future studies are needed to clarify this issue. Interestingly, no significant coupling was observed between alpha lateralization and BOLD in IPS in the current study. One possible reason is that the lateralization index was calculated as the difference in alpha power between the contra- and ipsilateral hemispheres. Given that IPS was inversely coupled with both contra- and ipsilateral alpha, the correlation between alpha power differences and BOLD in IPS is likely to be small.

Upper Alpha Versus Lower Alpha

It has been suggested that scalp-recorded alpha might be further divided into lower and upper alpha sub-bands and each sub-band is engaged in different cognitive and physiological processes (Klimesch 1999). To test whether our findings would be different for different alpha sub-bands, we also performed all our analyses using the following alpha sub-bands based on individual alpha frequencies (IAF): lower alpha (IAF-2 Hz to IAF) and upper alpha (IAF to IAF + 2 Hz). The results obtained by using different alpha sub-bands were found to be highly similar to those from the overall alpha band.

Limitations

The current study has the following limitations. First, although we observed strong postcue alpha lateralization among our participants, we found only a weak and not statistically significant negative association between alpha lateralization and reaction times in our study (i.e., stronger lateralization predicting faster response). The long cue-target intervals in our design, which are often used in fMRI studies of spatial attention to accommodate the sluggish BOLD response, might adversely impact the association between postcue alpha lateralization and behavior; prior work has shown that postcue alpha effects become weaker as the observation window is further moved away from cue onset (Zanto et al. 2011). Second, although the instructional cueing design is frequently used in spatial attention studies utilizing alpha as the dependent variable, it lacks a behavioral measure of attentional enhancement to ascertain whether participants sustained their attention throughout the relatively long cue-target period. This concern is mitigated by the observation of postcue alpha lateralization and increased BOLD responses to attended targets, indicating that subjects oriented attention according to the instructional cues and maintained a strong attention set during the cue-to-target interval. Finally, the coupling between EEG alpha and BOLD reported in this study are correlational in nature, and thus should be interpreted with caution. Our contention that the regions showing correlation with alpha are likely the regions exerting top-down modulation of alpha should be understood in conjunction with the current models of selective attention.

Conclusion

The current study contributes to our understanding of the top-down mechanisms of attention by providing evidence demonstrating the involvement of frontoparietal attentional control regions and executive control regions in the selective

biasing of sensory activity indexed by alpha oscillations during anticipatory attention. Our findings help to distinguish the differential roles of parietal and frontal regions within the frontoparietal attention network in modulating posterior alpha. By identifying regions whose BOLD responses were either inversely or positively coupled with alpha contralateral or ipsilateral to an attended spatial location, this study further provides evidence that visual attention mechanisms selectively enhance task-relevant visual cortex, while at the same time actively inhibit task-unrelated sensory and cognitive modalities. Further, a role of dACC and DLPFC in anticipatory attentional control is described, which is distinct from the influence of IPS in attentional control during anticipatory attention. Finally, the simultaneous EEG-fMRI technology has emerged as a powerful tool to examine the functional and anatomical substrates of time-resolved neural markers, including various components of event-related potentials and neural oscillatory activity (Laufs et al. 2003; Debener et al. 2005; Eichele et al. 2005; Scheeringa et al. 2011; Liu et al. 2012). As the current study demonstrates, it can provide both novel and corroborative evidence to complement other imaging and physiological methods.

Funding

This work was supported by the National Institutes of Health grants MH55714 to G.R.M. and MH097320 to M.D. and National Science Foundation grant BCS-1439188 to M.D. We thank Daesung Kang and Amy Trongnetrpunya for their assistance in data collection.

Notes

Conflict of Interest: None declared.

References

Aarts E, Roelofs A, van Turennout M. 2008. Anticipatory activity in anterior cingulate cortex can be independent of conflict and error likelihood. J Neurosci. 28:4671–4678.

Allen PJ, Josephs O, Turner R. 2000. A method for removing imaging artifact from continuous EEG recorded during functional MRI. Neuroimage. 12:230–239.

Allen PJ, Polizzi G, Krakow K, Fish DR, Lemieux L. 1998. Identification of EEG events in the MR scanner: the problem of pulse artifact and a method for its subtraction. Neuroimage. 8:229–239.

Anderson KL, Ding M. 2011. Attentional modulation of the somatosensory mu rhythm. Neuroscience. 180:165–180.

Armstrong K, Schafer R, Chang M, Moore T. 2012. Attention and action in the primate frontal eye fields. In: Mangun GR, editor. The Neuroscience of Attention: Attentional Control and Selection. New York: Oxford University Press. p. 151–166.

Barcelo F, Suwazono S, Knight RT. 2000. Prefrontal modulation of visual processing in humans. Nat Neurosci. 3:399–403.

Belouchrani A, Meraim KA, Cardoso JF, Moulines E. 1993. Second order blind separation of temporally correlated sources. In: Proc Int Conf on Digital Sig Proc, Cyprus.

Bengson JJ, Kelley TA, Zhang X, Wang JL, Mangun GR. (2014) Spontaneous neural fluctuations predict decisions to attend. J Cogn Neurosci. doi:10.1162/jocn_a_00650.

Bollimunta A, Chen Y, Schroeder CE, Ding M. 2008. Neuronal mechanisms of cortical alpha oscillations in awake-behaving macaques. J Neurosci. 28:9976–9988.

Bressler SL, Tang W, Sylvester CM, Shulman GL, Corbetta M. 2008. Top-down control of human visual cortex by frontal and parietal cortex in anticipatory visual spatial attention. J Neurosci. 28:10056–10061.

Briggs F, Mangun GR, Usrey WM. 2013. Attention enhances synaptic efficacy and the signal-to-noise ratio in neural circuits. Nature. 499:476–480.

Buckner RL, Andrews-Hanna JR, Schacter DL. 2008. The brain's default network: anatomy, function, and relevance to disease. Ann N Y Acad Sci. 1124:1–38.

Capotosto P, Babiloni C, Romani GL, Corbetta M. 2012. Differential contribution of right and left parietal cortex to the control of spatial attention: a simultaneous EEG–rTMS study. Cereb Cortex. 22:446–454.

Capotosto P, Babiloni C, Romani GL, Corbetta M. 2009. Frontoparietal cortex controls spatial attention through modulation of anticipatory alpha rhythms. J Neurosci. 29:5863–5872.

Chelazzi L, Duncan J, Miller EK, Desimone R. 1998. Responses of neurons in inferior temporal cortex during memory-guided visual search. J Neurophysiol. 80:2918–2940.

Chen Y, Dhamala M, Bollimunta A, Schroeder CE, Ding M. 2011. Current source density analysis of ongoing neural activity: theory and application. In: Vertes RP, Stackman RW, editors. Electrophysiological Recording Techniques. Totowa (NJ): Humana Press. p. 27–40.

Corbetta M, Kincade JM, Ollinger JM, McAvoy MP, Shulman GL. 2000. Voluntary orienting is dissociated from target detection in human posterior parietal cortex. Nat Neurosci. 3:292–297.

Corbetta M, Shulman GL. 2002. Control of goal-directed and stimulus-driven attention in the brain. Nat Rev Neurosci. 3:201–215.

Corbetta M, Shulman GL. 2011. Spatial neglect and attention networks. Annu Rev Neurosci. 34:569–599.

Crottaz-Herbette S, Menon V. 2006. Where and when the anterior cingulate cortex modulates attentional response: combined fMRI and ERP evidence. J Cogn Neurosci. 18:766–780.

Debener S, Ullsperger M, Siegel M, Fiehler K, von Cramon DY, Engel AK. 2005. Trial-by-trial coupling of concurrent electroencephalogram and functional magnetic resonance imaging identifies the dynamics of performance monitoring. J Neurosci. 25:11730–11737.

Delorme A, Makeig S. 2004. EEGLAB: an open source toolbox for analysis of single-trial EEG dynamics including independent component analysis. J Neurosci Methods. 134:9–21.

Dosenbach NU, Fair DA, Cohen AL, Schlaggar BL, Petersen SE. 2008. A dual-networks architecture of top-down control. Trends in Cogn Sci. 12:99–105.

Dosenbach NU, Visscher KM, Palmer ED, Miezin FM, Wenger KK, Kang HC, Burgund ED, Grimes AL, Schlaggar BL, Petersen SE. 2006. A core system for the implementation of task sets. Neuron. 50:799–812.

Eichele T, Specht K, Moosmann M, Jongsma MLA, Quiroga RQ, Nordby H, Hugdahl K. 2005. Assessing the spatiotemporal evolution of neuronal activation with single-trial event-related potentials and functional MRI. Proc Natl Acad Sci USA. 102:17798–17803.

Fox MD, Zhang D, Snyder AZ, Raichle ME. 2009. The global signal and observed anticorrelated resting state brain networks. J Neurophysiol. 101:3270–3283.

Foxe JJ, Simpson GV, Ahlfors SP. 1998. Parieto-occipital approximately 10 Hz activity reflects anticipatory state of visual attention mechanisms. Neuroreport. 9:3929–3933.

Fu KMG, Foxe JJ, Murray MM, Higgins BA, Javitt DC, Schroeder CE. 2001. Attention-dependent suppression of distracter visual input can be cross-modally cued as indexed by anticipatory parieto–occipital alpha-band oscillations. Cogn Brain Res. 12:145–152.

Gitelman DR, Nobre AC, Parrish TB, LaBar KS, Kim YH, Meyer JR, Mesulam MM. 1999. A large-scale distributed network for covert spatial attention Further anatomical delineation based on stringent behavioural and cognitive controls. Brain. 122:1093–1106.

Grent-'t-Jong T, Boehler CN, Kenemans JL, Woldorff MG. 2011. Differential functional roles of slow-wave and oscillatory-alpha activity in visual sensory cortex during anticipatory visual–spatial attention. Cereb Cortex. 21:2204–2216.

Haegens S, Händel BF, Jensen O. 2011. Top-down controlled alpha band activity in somatosensory areas determines behavioral performance in a discrimination task. J Neurosci. 31:5197–5204.

Haegens S, Osipova D, Oostenveld R, Jensen O. 2010. Somatosensory working memory performance in humans depends on both engagement and disengagement of regions in a distributed network. Hum Brain Mapp. 31:26–35.
Händel BF, Haarmeier T, Jensen O. 2011. Alpha oscillations correlate with the successful inhibition of unattended stimuli. J Cogn Neurosci. 23:2494–2502.
Heinze HJ, Mangun GR, Burchert W, Hinrichs H, Scholz M, Münte TF, Gös A, Scherg M, Johannes S, Hundeshagen H et al. 1994. Combined spatial and temporal imaging of brain activity during visual selective attention in humans. Nature. 372:543–546.
Hilgetag CC, Théoret H, Pascual-Leone A. 2001. Enhanced visual spatial attention ipsilateral to rTMS-induced "virtual lesions" of human parietal cortex. Nat Neurosci. 4:953–957.
Holmes AP, Blair RC, Watson G, Ford I. 1996. Nonparametric analysis of statistic images from functional mapping experiments. J Cereb Blood Flow Metab. 16:7–22.
Hopf JM, Mangun GR. 2000. Shifting visual attention in space: an electrophysiological analysis using high spatial resolution mapping. Clin Neurophysiol. 111:1241–1257.
Hopfinger JB, Buonocore MH, Mangun GR. 2000. The neural mechanisms of top-down attentional control. Nat Neurosci. 3:284–291.
Hung J, Driver J, Walsh V. 2005. Visual selection and posterior parietal cortex: effects of repetitive transcranial magnetic stimulation on partial report analyzed by Bundesen's theory of visual attention. J Neurosci. 25:9602–9612.
Jensen O, Mazaheri A. 2010. Shaping functional architecture by oscillatory alpha activity: gating by inhibition. Front Hum Neurosci. 4:186.
Kastner S, Pinsk MA, Weerd PD, Desimone R, Ungerleider LG. 1999. Increased activity in human visual cortex during directed attention in the absence of visual stimulation. Neuron. 22:751–761.
Kelly SP, Gomez-Ramirez M, Foxe JJ. 2009. The strength of anticipatory spatial biasing predicts target discrimination at attended locations: a high-density EEG study. Eur J Neurosci. 30:2224–2234.
Kelly SP, Lalor EC, Reilly RB, Foxe JJ. 2006. Increases in alpha oscillatory power reflect an active retinotopic mechanism for distracter suppression during sustained visuospatial attention. J Neurophysiol. 95:3844–3851.
Klimesch W. 1999. EEG alpha and theta oscillations reflect cognitive and memory performance: a review and analysis. Brain Res Rev. 29:169–195.
Klimesch W, Sauseng P, Hanslmayr S. 2007. EEG alpha oscillations: the inhibition–timing hypothesis. Brain Res Rev. 53:63–88.
Laufs H, Kleinschmidt A, Beyerle A, Eger E, Salek-Haddadi A, Preibisch C, Krakow K. 2003. EEG-correlated fMRI of human alpha activity. Neuroimage. 19:1463–1476.
Liu Y, Huang H, McGinnis-Deweese M, Keil A, Ding M. 2012. Neural substrate of the late positive potential in emotional processing. J Neurosci. 32:14563–14572.
Luck SJ, Chelazzi L, Hillyard SA, Desimone R. 1997. Neural mechanisms of spatial selective attention in areas V1, V2, and V4 of macaque visual cortex. J Neurophysiol. 77:24–42.
MacDonald AW, Cohen JD, Stenger VA, Carter CS. 2000. Dissociating the role of the dorsolateral prefrontal and anterior cingulate cortex in cognitive control. Science. 288:1835–1838.
Mayhew SD, Ostwald D, Porcaro C, Bagshaw AP. 2013. Spontaneous EEG alpha oscillation interacts with positive and negative BOLD responses in the visual–auditory cortices and default-mode network. Neuroimage. 76:362–372.
Mesulam MM. 1981. A cortical network for directed attention and unilateral neglect. Ann Neurol. 10:309–325.
Mesulam MM. 1999. Spatial attention and neglect: parietal, frontal and cingulate contributions to the mental representation and attentional targeting of salient extrapersonal events. Phil Trans R Soc Lond B. 354:1325–1346.
Miller EK, Buschman TJ. 2013. Cortical circuits for the control of attention. Curr Opin Neurobiol. 23:216–222.
Mitzdorf U. 1985. Current source-density method and application in cat cerebral cortex: investigation of evoked potentials and EEG phenomena. Physiol Rev. 65:37–100.
Mo J, Liu Y, Huang H, Ding M. 2013. Coupling between visual alpha oscillations and default mode activity. Neuroimage. 68:112–118.
Moore T, Armstrong KM. 2003. Selective gating of visual signals by microstimulation of frontal cortex. Nature. 421:370–373.
Moore T, Fallah M. 2004. Microstimulation of the frontal eye field and its effects on covert spatial attention. J Neurophysiol. 91:152–162.
Moran J, Desimone R. 1985. Selective attention gates visual processing in the extrastriate cortex. Science. 229:782–784.
Navon D, Gopher D. 1979. On the economy of the human-processing system. Psychol Rev. 86:214–253.
Nichols TE, Holmes AP. 2001. Nonparametric permutation tests for functional neuroimaging: a primer with examples. Hum Brain Map. 15:1–25.
O'Connor DH, Fukui MM, Pinsk MA, Kastner S. 2002. Attention modulates responses in the human lateral geniculate nucleus. Nat Neurosci. 5:1203–1209.
Posner MI. 1980. Orienting of attention. Q J Exp Psychol. 32:3–25.
Rajagovindan R, Ding M. 2011. From prestimulus alpha oscillation to visual-evoked response: an inverted-U function and its attentional modulation. J Cogn Neurosci. 23:1379–1394.
Romei V, Brodbeck V, Michel C, Amedi A, Pascual-Leone A, Thut G. 2008. Spontaneous fluctuations in posterior α-band EEG activity reflect variability in excitability of human visual areas. Cereb Cortex. 18:2010–2018.
Ruff CC, Bestmann S, Blankenburg F, Bjoertomt O, Josephs O, Weiskopf N, Deichmann R, Driver J. 2008. Distinct causal influences of parietal versus frontal areas on human visual cortex: evidence from concurrent TMS–fMRI. Cereb Cortex. 18:817–827.
Ruff CC, Blankenburg F, Bjoertomt O, Bestmann S, Freeman E, Haynes JD, Rees G, Josephs O, Deichmann R, Driver J. 2006. Concurrent TMS-fMRI and psychophysics reveal frontal influences on human retinotopic visual cortex. Curr Biol. 16:1479–1488.
Sakai K. 2008. Task set and prefrontal cortex. Annu Rev Neurosci. 31:219–245.
Sauseng P, Feldheim JF, Freunberger R, Hummel FC. 2011. Right prefrontal TMS disrupts interregional anticipatory EEG alpha activity during shifting of visuospatial attention. Front Psychol. 2(241):1–9.
Sauseng P, Klimesch W, Stadler W, Schabus M, Doppelmayr M, Hanslmayr S, Gruber WR, Birbaumer N. 2005. A shift of visual spatial attention is selectively associated with human EEG alpha activity. Eur J Neurosci. 22:2917–2926.
Scheeringa R, Fries P, Petersson KM, Oostenveld R, Grothe I, Norris DG, Hagoort P, Bastiaansen MCM. 2011. Neuronal dynamics underlying high- and low-frequency EEG oscillations contribute independently to the human BOLD signal. Neuron. 69:572–583.
Selemon LD, Goldman-Rakic PS. 1988. Common cortical and subcortical targets of the dorsolateral prefrontal and posterior parietal cortices in the rhesus monkey: evidence for a distributed neural network subserving spatially guided behavior. J Neurosci. 8:4049–4068.
Shulman GL, McAvoy MP, Cowan MC, Astafiev SV, Tansy AP, d'Avossa G, Corbetta M. 2003. Quantitative analysis of attention and detection signals during visual search. J Neurophysiol. 90:3384–3397.
Szczepanski SM, Konen CS, Kastner S. 2010. Mechanisms of spatial attention control in frontal and parietal cortex. J Neurosci. 30:148–160.
Thut G, Nietzel A, Brandt SA, Pascual-Leone A. 2006. α-band electroencephalographic activity over occipital cortex indexes visuospatial attention bias and predicts visual target detection. J Neurosci. 26:9494–9502.
Thut G, Nietzel A, Pascual-Leone A. 2005. Dorsal posterior parietal rTMS affects voluntary orienting of visuospatial attention. Cereb Cortex. 15:628–638.
Tootell RBH, Hadjikhani N, Hall EK, Marrett S, Vanduffel W, Vaughan JT, Dale AM. 1998. The retinotopy of visual spatial attention. Neuron. 21:1409–1422.
Van Voorhis S, Hillyard SA. 1977. Visual evoked potentials and selective attention to points in space. Percept Psychophys. 22:54–62.
Vossel S, Weidner R, Driver J, Friston KJ, Fink GR. 2012. Deconstructing the architecture of dorsal and ventral attention systems with dynamic causal modeling. J Neurosci. 32:10637–10648.

Walsh BJ, Buonocore MH, Carter CS, Mangun GR. 2011. Integrating conflict detection and attentional control mechanisms. J Cogn Neurosci. 23:2211–2221.
Wen X, Liu Y, Yao L, Ding M. 2013. Top-down regulation of default mode activity in spatial visual attention. J Neurosci. 33: 6444–6453.
Worden MS, Foxe JJ, Wang N, Simpson GV. 2000. Anticipatory biasing of visuospatial attention indexed by retinotopically specific alpha-band electroencephalography increases over occipital cortex. J Neurosci. 20(RC63):1–6.
Yamagishi N, Callan DE, Goda N, Anderson SJ, Yoshida Y, Kawato M. 2003. Attentional modulation of oscillatory activity in human visual cortex. Neuroimage. 20:98–113.
Zanto TP, Pan P, Liu H, Bollinger J, Nobre AC, Gazzaley A. 2011. Age-related changes in orienting attention in time. J Neurosci. 31:12461–12470.